Pharmacological Research 189 (2023) 106683

Contents lists available at ScienceDirect

Pharmacological Research

journal homepage: www.elsevier.com/locate/yphrs

Cannabidiol alters mitochondrial bioenergetics via VDAC1 and triggers cell death in hormone-refractory prostate cancer

Ali Mokhtar Mahmoud [a], Magdalena Kostrzewa [a], Viviana Marolda [a], Marianna Cerasuolo [b], Federica Maccarinelli [c], Daniela Coltrini [c], Sara Rezzola [c], Arianna Giacomini [c], Maria Pina Mollica [d], Andrea Motta [a], Debora Paris [a], Antonio Zorzano [e,f,g], Vincenzo Di Marzo [a,h], Roberto Ronca [c,*], Alessia Ligresti [a,**]

[a] National Research Council of Italy, Institute of Biomolecular Chemistry, Pozzuoli, Italy
[b] University of Portsmouth, School of Mathematics and Physics, Hampshire PO1 3HF, UK
[c] University of Brescia, Department of Molecular and Translational Medicine, Brescia, Italy
[d] Department of Biology, University of Naples Federico II, Naples, Italy
[e] Institute for Research in Biomedicine, (IRB Barcelona), The Barcelona Institute of Science and Technology, Barcelona, Spain
[f] Departament de Bioquímica i Biomedicina Molecular, Facultat de Biologia, Universitat de Barcelona, Barcelona, Spain
[g] Centro de Investigación Biomédica en Red de Diabetes y Enfermedades Metabólicas Asociadas (CIBERDEM) Instituto de Salud Carlos III, Spain
[h] Centre de Recherche de l'Institut de Cardiologie et Pneumologie de Quebéc (CRIUCPQ) et Institut sur la Nutrition et les Aliments Fonctionnels (INAF), Centre NUTRISS, Department of Medicine and School of Nutrition, Université Laval, Quebec City, Canada

ARTICLE INFO

Keywords:
Mitochondrial bioenergetics
CBD
VDAC1
Hormone refractory prostate cancer
Phytocannabinoids

ABSTRACT

In spite of the huge advancements in both diagnosis and interventions, hormone refractory prostate cancer (HRPC) remains a major hurdle in prostate cancer (PCa). Metabolic reprogramming plays a key role in PCa oncogenesis and resistance. However, the dynamics between metabolism and oncogenesis are not fully understood. Here, we demonstrate that two multi-target natural products, cannabidiol (CBD) and cannabigerol (CBG), suppress HRPC development in the TRansgenic Adenocarcinoma of the Mouse Prostate (TRAMP) model by reprogramming metabolic and oncogenic signaling. Mechanistically, CBD increases glycolytic capacity and inhibits oxidative phosphorylation in enzalutamide-resistant HRPC cells. This action of CBD originates from its effect on metabolic plasticity via modulation of VDAC1 and hexokinase II (HKII) coupling on the outer mitochondrial membrane, which leads to strong shifts of mitochondrial functions and oncogenic signaling pathways. The effect of CBG on enzalutamide-resistant HRPC cells was less pronounced than CBD and only partially attributable to its action on mitochondria. However, when optimally combined, these two cannabinoids exhibited strong anti-tumor effects in TRAMP mice, even when these had become refractory to enzalutamide, thus pointing to their therapeutical potential against PCa.

1. Introduction

The number of men living with PCa is increasing around the world with over 20 million expected in 2024 [1]. Since androgens play an essential role in PCa growth and most types of PCa at early diagnosis are androgen-dependent [2], the inhibition of androgen (AR) signaling represents the first line of therapy, and results in initial tumor regression. However, tumor cells adapt to low androgen signaling and develop resistance to treatment leading to the so-called castration resistant phase (CRPC) characterized by AR signaling reactivation [3]. AR signaling inhibitors, like enzalutamide, significantly improve CRPC patient survival and quality of life [4], but their effect is not long lasting, and tumor ultimately relapses as hormone-refractory prostate cancer (HRPC), which is no longer treatable by any known form of hormonal

Abbreviations: HRPC, hormone refractory prostate cancer; PCa, prostate cancer; CBD, cannabidiol; CBG, cannabigerol; TRAMP, TRansgenic Adenocarcinoma of the Mouse Prostate; AR, androgen receptor.

* Corresponding author.
** Correspondence to: University of Brescia, viale Europa 11, 25123 Brescia, Italy.
E-mail addresses: roberto.ronca@unibs.it (R. Ronca), aligresti@icb.cnr.it (A. Ligresti).

https://doi.org/10.1016/j.phrs.2023.106683
Received 24 October 2022; Received in revised form 18 January 2023; Accepted 30 January 2023
Available online 1 February 2023

therapy [5]. Due to the lack of alternative therapies, unveiling new druggable pathways in addition to hormonal therapy is eagerly required to improve the clinical outcome. Indeed, metabolic reprogramming represents a hallmark of cancer growth that is gaining great relevance due to the numerous studies that strongly correlate the up-regulation of glucose metabolism and resistance to hormone therapy [6,7]. In this perspective, the mitochondrion is the prominent organelle governing the main metabolic pathways as well as oncogenic and cell death signals [8].

Plant-derived cannabinoids have been used for many decades as palliative agents for cancer patients, and different such compounds and cannabinoid-based pharmaceutical drugs have been the subject of intensive research for their potential antitumor activity [9–14]. Even though much evidence can be found in the literature on the ability of these compounds to induce cell death by various pathways in PCa [11, 15–17], more research is needed to understand their exact molecular targets and mechanism(s) of action. Meanwhile, a phase I/Ib study is determining the safety and effectiveness of Epidiolex (cannabidiol) in biochemically recurrent PCa patients [18]. We previously reported that non-psychoactive cannabinoids inhibit PCa growth in vitro and in vivo (in xenograft tumors) via a combination of cannabinoid receptor-independent cellular and molecular mechanisms. The rank order of potency showed CBD as the most potent among the purified cannabinoids, followed by CBG in both androgen-sensitive and androgen-insensitive neuroendocrine-like PCa cells [11]. To explore further the efficacy of cannabinoids in a pre-clinical model that can mimic more accurately the human disease, we recently characterized the acquired resistance to the second-generation androgen receptor antagonist enzalutamide in the multistage transgenic TRAMP mouse model of prostate cancer. Our integrated approach, merging mathematical modeling with experimental data, examined the in vitro and in vivo evolution of PCa resistance to enzalutamide, leading to the implementation of a "TRAMP-based platform" to be exploited for the validation of new therapeutic strategies for PCa [16].

In the present study, by using the TRAMP model, we studied the efficacy of a combination (1:1) of cannabinoids (CBD:CBG) not only in the early and advanced phase of PCa, but especially in the HRPC phase. Furthermore, we investigated the mechanistic aspects of CBD action,

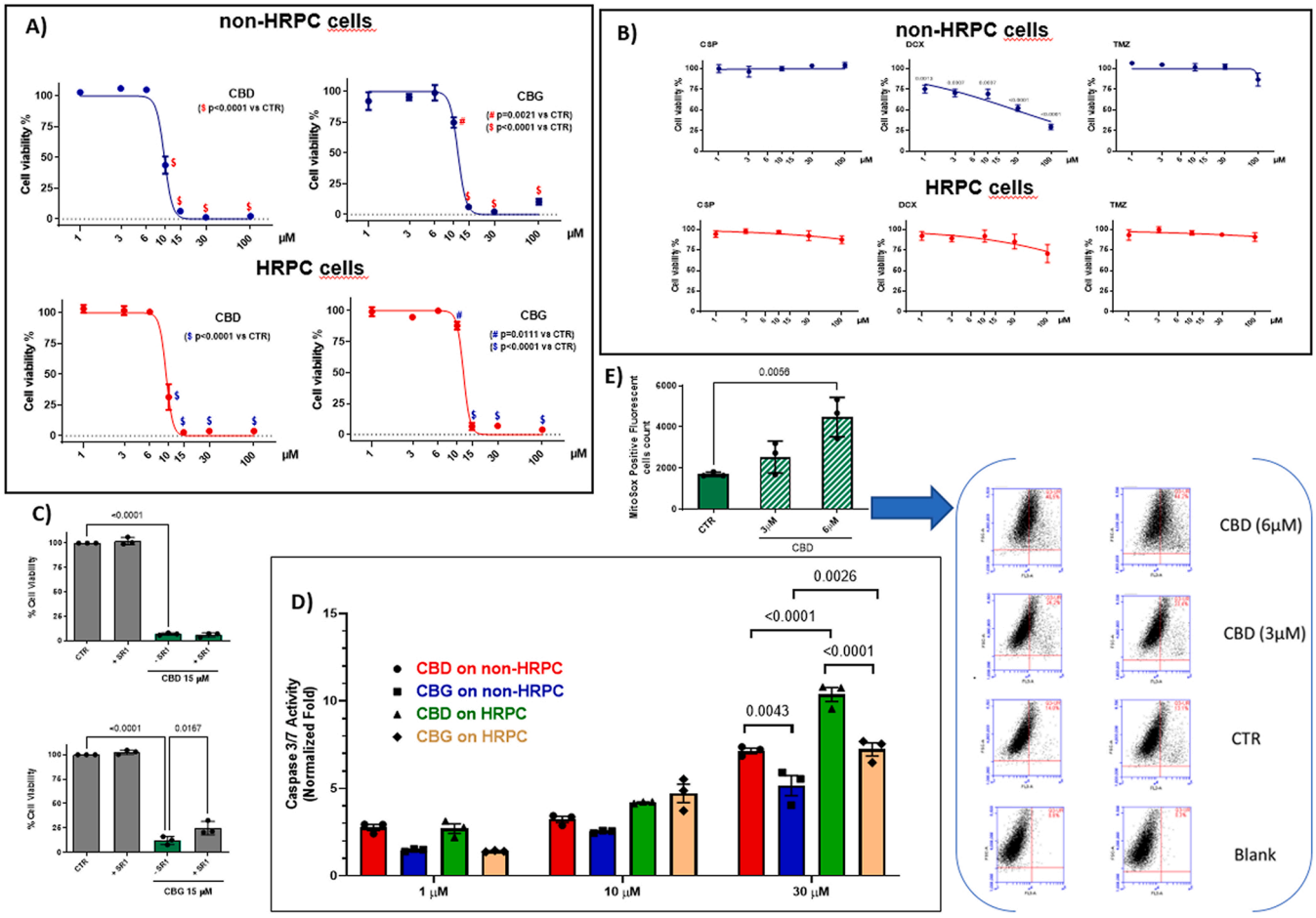

Fig. 1. CBD- and CBG- induced cell death in non-HRPC and HRPC cells. Effect on cell viability after 24 h treatment with purified cannabinoids (A) or main chemotherapy drugs (B) used in clinics (CSP: cisplatin; DCX: Docetaxel; TMZ: Temozolomide). Effect on cell viability of an active dose of CBG in the presence of 1 μM SR1 (SR141716A), a CB1 receptor antagonist (C). Effect on caspase activation (D) in cells treated for 3 h. Representative flow cytometry plots illustrating the determination of mitochondrial superoxide production in HRPC cells after 24 h by MitoSOX-based assay (E). All data are reported as mean ± SD of three independent experiments run in triplicate. Data were analyzed using ordinary one-way ANOVA followed by the appropriate multiple comparison test (Dunnett for panel 1 A, 1B and 1E, Sidak for panel 1 C). Three-way ANOVA followed by Tukey post-hoc test was applied in panel 1D to analyze data (difference intra/inter treatments per cell phenotype). Stats for panel 1 A: F (7,16) = 144 and 363 (with $p < 0.0001$ for CBD on HRPC and non-HRPC, respectively); 413 and 130 (with $p < 0.0001$ for CBG on HRPC and non-HRPC, respectively). Stats for panel 1B: F(5,12)= 1.430 and 0.5884 (with $p = 0.0438$ and 0.7092 for CSP on HRPC and non-HRPC, respectively); 1.936 and 32.74 (with $p = 0.1617$ and <0.0001 for DCX on HRPC and non-HRPC, respectively); 0.9791 and 3.249 (with $p = 0.4690$ and 0.0438 for TMZ on HRPC and non-HRPC, respectively). Stats for panel 1 C: F(3,8)= 1812 and 406 (with $p < 0.0001$ for CBD and CBG, respectively). Stats for panel 1D: F(1,24)= 57.72 (CBD vs CBG inter-treatment, $p < 0.0001$); F(2,4)= 228.9 and 1128 (CBD and CBG intra-treatment, respectively with $p < 0.0001$). Stats for panel 1E: F(2,6)= 11.9 with $p = 0.0081$.

focusing on its modification of mitochondrial function. Our findings collectively support the existence of metabolic and oncogenic vulnerabilities in HRPC that can be used as novel therapeutical targets and support the need of clinical investigations aimed at validating the combined use of CBD and CBG in adjuvant therapy for this lethal phase of the disease.

2. Results

2.1. CBD and CBG induce cell death in non-HRPC and HRPC cells via non canonical cannabinoid molecular targets

To assess the effect of cannabinoids on PCa cell growth depending on the pathological context, we tested the effect of CBD and CBG on cell death in both naïve non-HRPC TRAMP-C2 cells and enzalutamide-resistant HRPC TRAMP-C2 cells originated by long term culturing in the presence of enzalutamide [16]. As shown in Fig. 1A treatments with CBD and CBG were active on both naïve non-HRPC cells (IC_{50} values of 11 ± 0.48 μM and 13 ± 0.53 μM, respectively) and HRPC cells (IC_{50} values of 10 ± 1.00 μM for CBD and 14 ± 0.21 μM for CBG), suggesting that these two molecules can induce cell death in PCa cells regardless of their sensitivity to androgen signaling inhibitors or dependence on hormones. Differently from cannabinoids, canonical chemotherapeutics (cisplatin, docetaxel and temozolomide did not show any relevant effect on these PCa cells both in naïve and HRPC status, with the only exception of docetaxel that exhibited a cytotoxic effect (IC_{50} of 32 ± 12.08 μM) on non-HRPC TRAMP-C2 cells (Fig. 1B). Given this promising effect of CBD and CBG, we verified if their action was mediated by their canonical targets. To this purpose, we treated both non-HRPC and HRPC cells with an active dose of cannabinoids (15 μM) after 1 h pre-incubation with a selective antagonist for cannabinoid receptors (CB1 and CB2), transient receptor potential channels (TRPV1, TRPV4, TRPA1) or nuclear receptors (PPARγ). The concentrations of the antagonists were selected in pilot experiments (data not shown) based on the maximum inactive dose and on the potency of the reported ligand for the correspondent receptor/channel. As shown in Fig. S1, none of these antagonists was able to prevent the effect of CBD and CBG on either naïve non-HRPC or HRPC cells, with only a partial effect being observed in CBG-treated HRPC cells after pre-incubation with the CB1 antagonist SR141716A (Fig. 1C).

Regarding apoptosis, instead, our analysis revealed that HRPC cells were more sensitive than non-HRPC cells to the pro-apoptotic effect of cannabinoids and that the activation of caspases was significantly greater in CBD-treated compared to CBG-treated cells (Fig. 1D). The difference among treatments was statistically relevant only at the highest concentration tested (30 μM), which was possibly due to the short-time incubation (3 h) considered. Indeed, after a longer treatment (24 h), mRNA expression of BNIP3 (Bcl-2 interacting protein 3), a key regulator of hypoxia-induced apoptosis was significantly up-regulated by a lower concentration (6 μM) of CBD in HRPC cells (Fig. S2A). On the other hand, CBG at the same concentration showed the opposite effect (Fig. S2B). Mitochondria play a central role in effector caspase activation as both known apoptotic pathways induce mitochondrial outer membrane permeabilization and the release of pro-apoptotic signals from the mitochondria to the cytoplasm. A preliminary analysis revealed that mitochondria organization was different in the two cell lines, with HRPC cells showing smaller mitochondrial mass compared to naive cells (Fig. S3A and S3B). A 3D reconstruction of mitochondrial architecture with the aid of MitoKondrY macro for ImageJ [19] confirmed the existence of different features in the two cell phenotypes by showing an increased fragmentation and a reduced network capability in HRPC cells with respect to non-HRPC cells (Fig. S3C-E). In HRPC cells, treatment with CBD at 6 μM significantly increases mtROS production (Fig. 1E). Interestingly, the addition of the antioxidant α-Tocopherol completely reverted the effect of CBD on cell viability and on the activation of caspases 3 and 7 in HRPC cells (Fig. S4A-B).

2.2. CBD and CBG exert cell-dependent divergent effects on glycolytic capacity and maximal oxidative phosphorylation capacity

The effect of CBD and CBG on the main metabolic pathways in both cell types was investigated. First, we applied Orthogonal Projections to Latent Structures Discriminant Analysis (OPLS-DA) to NMR spectra to investigate cell metabolic profiles in response to treatments. In non-HRPC cells, a complete class separation with a clear distinction between CBD and CBG treatment was observed, as well as with respect to the control/vehicle (CTR). The model suggested that CBD treatment induces different metabolic alterations compared to CBG treatment (Fig. 2A and S5-S6). A consistent class separation among groups was observed in HRPC cells as well, and the up-regulated metabolites in HRPC cells treated with CBD (i.e., pyruvate and lactate) suggested increased glycolytic capacity (Fig. 2A and S7-S8). Then the effect of both cannabinoids on glycolysis and oxidative phosphorylation was measured by quantifying the oxygen consumption rate (OCR) and extracellular acidification rate (ECAR) using Seahorse extracellular flux analyzer (Fig. 2B). In agreement with the NMR analysis, in non-HRPC cells CBD did not affect the mitochondrial oxidative phosphorylation capacity, and only slightly increased the glycolytic capacity, while CBG changed neither OCR nor ECAR (Fig. S9). In HRPC cells, CBD increased glycolytic capacity and inhibited maximal capacity of oxidative phosphorylation (Fig. 2B) while CBG did not significantly change ECAR and showed a trend for increased OCR (Fig. 2B). Accordingly, in HRPC cells, CBD significantly up-regulated mRNA expression of genes involved in cell metabolism like AMP-activated protein Kinase (AMPK), glutaminase (GLS), lactate dehydrogenase (LDH), Hexokinases-II (HK2) and pyruvate dehydrogenase kinase (PDK1) (Fig. S10). Altogether these data indicate that the two cannabinoids provoke divergent effects at the metabolic level depending on the PCa phenotype under investigation.

2.3. CBD promotes mitochondrial dysfunction in HRPC cells

Since in HRPC cells only CBD showed a significant effect on bioenergetics processes, we wanted to examine whether mitochondria targeting is a direct and early event of CBD-induced cell death and how CBD-induced regulation of mitochondrial activity is linked with its effect on glycolysis. We measured the ATP respiration rate in HRPC cells, and we found that a 24-hour treatment with CBD significantly decreased mitochondrial ATP production (Fig. 3A and B). We assessed by Western blot the effect of CBD treatment (3 μM and 6 μM, 24 h) on the levels of key proteins regulating mitochondrial dynamics and we found that CBD significantly reduced the level of fusion-related protein MFN-1 (Fig. S11A) while significantly increasing the levels of fission-related FIS-1 (Fig. S11B). To gain new clues on how CBD modulates mitochondrial morphology, we first assessed its effect on mitochondrial shape by Super-Resolution Confocal Microscopy and found that, after a 3-hour treatment at 6 μM, CBD-treated cells exhibited a fragmented mitochondrial morphology in comparison with untreated (CTR) cells. Thus, confirming that CBD can promote a higher mitochondrial fission rate in HRPC cells (Fig. 3C). Image analysis indicated that CBD promoted a concentration-dependent decrease of both mitochondrial membrane potential and mitochondrial mass after 24-hour treatment (Fig. 3D and E). For in-depth analysis of mitochondrial features, the mitochondrial architecture was reconstructed in 3D (Fig. 3F) with the aid of MitoKondrY macro for ImageJ as previously described [19] and its connectivity by means of network capability along with its promotion of fission were quantified. Morphological analysis indicated that a 3-hour treatment at 6 μM with CBD significantly reduced connectivity (Fig. 3G), while increasing fragmentation (Fig. 3H). Notably, in agreement with the early pro-apoptotic action shown in Fig. 1, we found a consistent accumulation of CBD in a VDAC-1 enriched mitochondrial fraction of HRPC cells, already after 3 h of treatment (Fig. S12A and Fig. S12B).

Electron microscopy analysis confirmed that a short treatment with

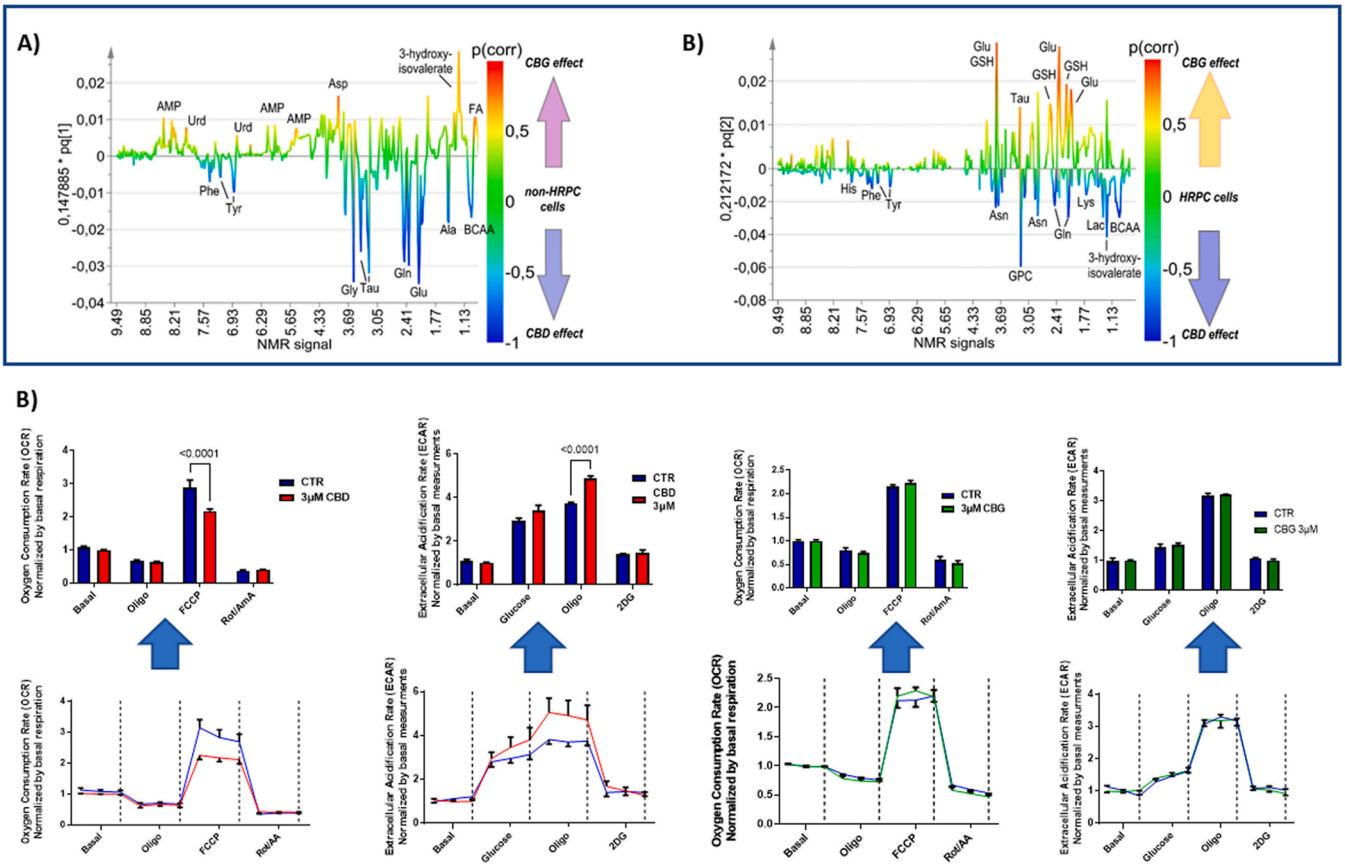

Fig. 2. Effect of CBD and CBG on cell bioenergetics in non-HRPC and HRPC cells. (**A**) S-line plot generated by multivariate data analysis of the NMR acquired metabolic profiles. In both phenotypes (non-HRPC and HRPC cells), metabolic changes (positive changes oriented along with the color-coded arrows) in CBD-treated cells compared with CBG-treated cells are shown in blue/red as the positive/negative correlations. (**B**) Effect of CBD and CBG on oxygen consumption rate (OCR) and extracellular acidification rate (ECAR) in HRPC cells. Mitochondria respiration and glycolysis flux rate were measured by bioenergetic analysis using Seahorse XF stress kits. Data are shown as mean ± SEM of 3 independent experiments (run in quadruplicate) normalized to the basal measurement. For statistical analysis, two-way ANOVA followed by Sidak multiple comparisons test was used to analyze the bar plots of each correspondent tracing. Stats: F(3,16)= 22.79 and 700.3 (CBD on OCR interaction and respiratory state, respectively); 0.4291 and 617.2 (CBD on ECAR interaction and respiratory state, respectively).

CBD (6 μM, 3 h) induced significant changes of morphology and produced mitochondrial swelling followed by cristae fragmentation (Fig. 4A and B). High-resolution respirometry studies in permeabilized HRPC cells demonstrated that a shorter exposure to the same CBD treatment (6 μM, 3 h) reduced the maximal respiration capacity and inhibited both Complex I-II and Complex IV (Fig. 4C and D).

2.4. *CBD-induced mitochondrial dysfunction modulates oncogenic signaling and induces autophagy in HRPC cells*

We hypothesized that in HRPC cells the effect of CBD on the main metabolic pathways alters the expression of relevant transcription factors and oncogenic signaling. Therefore, we tested mRNA and protein levels after CBD treatment (6 μM, 24 h) and found significantly up-regulated mRNA expression of *cMyc*, *PTEN* and *HIF-1α* (Fig. 5A). At the protein level, the effect on PTEN was confirmed, and the effect of CBD on p53 and AKT activation/phosphorylation was tested. A significant effect was only observed on pAkt (Fig. 5B). In agreement with the role of the PI3K/Akt/mTOR pathway in the modulation of autophagy, we confirmed that the inhibition by CBD of Akt activation promoted autophagy in HRPC cells by increasing ULK1 mRNA level (Fig. 5C) and LC3II protein (Fig. 5D).

2.5. *VDAC1 binding is essential for CBD-induced effects on mitochondria in HRPC cells*

CBD is reported to bind VDAC1, a key protein that regulates both cell metabolism and apoptosis at the mitochondrial level [20,21]. To investigate whether CBD-induced mitochondrial actions are mediated by this channel, we tested the effect of CBD on cell fate in the presence of DIDS, a VDAC1 oligomerization inhibitor. We found that pre-incubation with DIDS significantly reverted not only the inhibition of cell viability triggered by CBD, but also the activation of caspase 3 and 7 and consequently the effect on mitochondrial ATP (Fig. 6A-6 C). Moreover, CBD induced a time-dependent recruitment of proteins that can oligomerize with VDAC1 at the mitochondrial level. In particular, we found a significant increase of HK-II and BAX over time (Fig. 6D-6 F).

2.6. *CBD and CBG inhibit tumor growth in vivo and prevent occlusive and antagonist effects with therapy in combined treatments*

Given the actions exerted by CBD and CBG in vitro, we moved on to in vivo validation of their antitumor activity. We started with exploring the effect of CBD or CBG in a single dose (75 mg/kg) and in a 1:1 combined treatment using half of the single dose of each (37.5 +37.5 mg/kg) in a short-term *ex vivo* experiment by injecting non-HRPC cells subcutaneously in an alginate matrix [22] and treating/analyzing tumors when cells begin to create a favorable environment to grow. As shown in Fig. S13, all treatments (single and in combination)

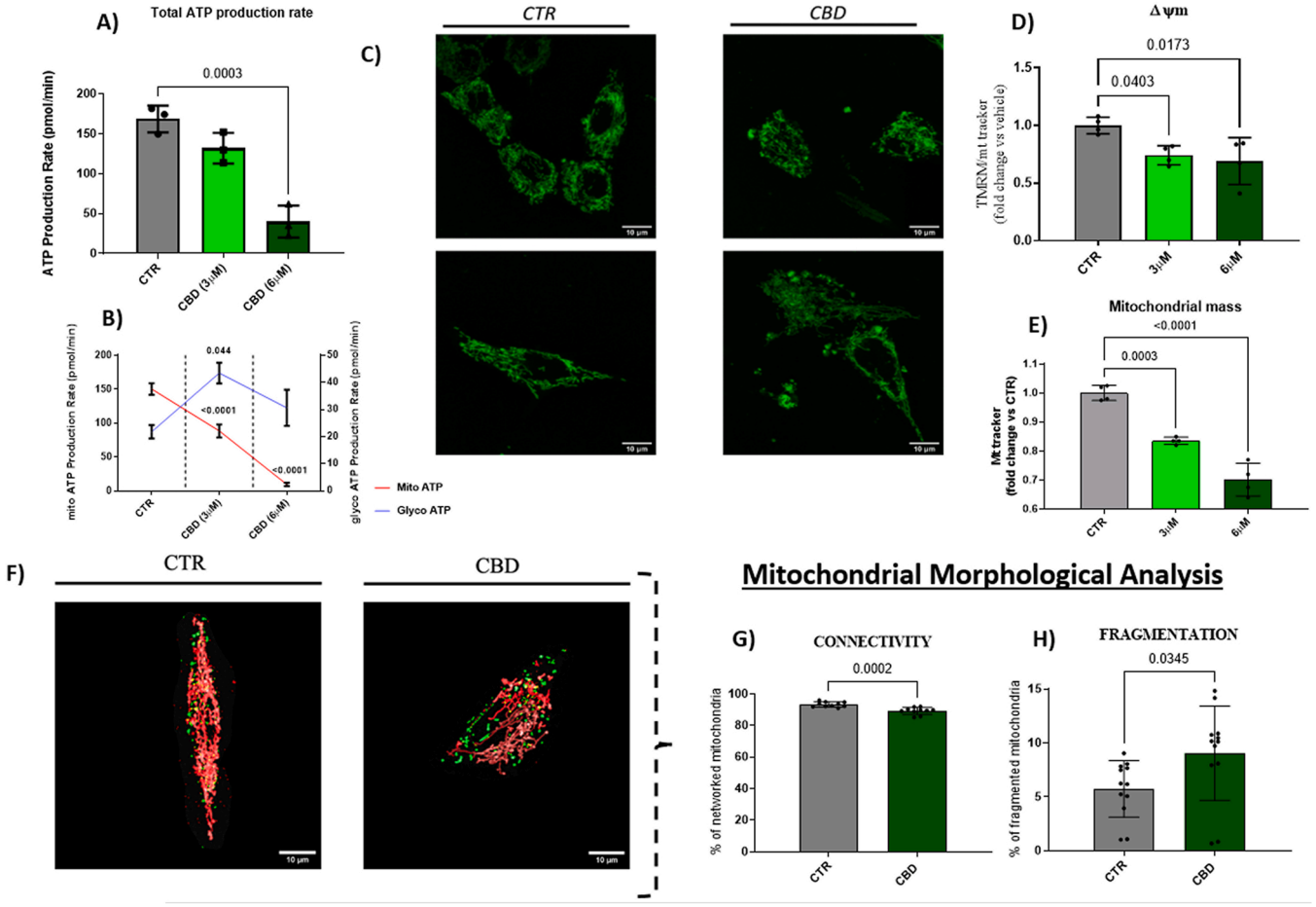

Fig. 3. CBD targeting of mitochondria is an early event promoting mitochondrial dysfunction in HRPC cells. Determination of ATP production in HRPC cells by Seahorse XF Real-Time ATP Rate Assay Kit. Total (**A**) and fractionated (**B**) ATP rate between mitochondria respiration-dependent and cytoplasmic glycolysis-dependent are reported. Two representative images per group of a 3-hour treatment with 6 μM CBD acquired by super-resolution confocal microscopy after loading cells with Mitotracker fluorescence dye (50 nM, 30 min) are reported (**C**). Determination of CBD effect on mitochondrial membrane potential ΔΨm (**D**) and mitochondrial mass (**E**) by FACS. 3D reconstruction of mitochondrial architecture after a 3-hour treatment with 6 μM CBD acquired by super-resolution confocal microscopy (**F**) together with the quantification of mitochondrial architecture (**G**, **H**). Normally distributed data are reported as mean ± SEM of at least 3 independent experiments run in triplicate: n = 3 in panel 3 A; n = 4 in panels 3D, 3E, 3 G and 3 H; n = 14 for CTR and n = 10 for CBD treated samples in panel 3B). For statistical analysis, unpaired t-Test was used to make comparisons between the groups was used for panel G (t = 4.644, df=18) and for panel H (t = 2.253, tf=22). Ordinary one-way or two-way (vs CTR, panel 3B) ANOVA followed by Dunnett's multiple comparison test was used with F(2, 6) = 37.34 and p = 0.0004 [panel A]; F (2,9)= 6.197 (p = 0.0203) and 67.08 (p < 0.0001 [panel D and E, respectively]; F(2,60)= 67.69 and 52.80 (interaction and treatment, respectively [panel 3B] with p < 0.0001; F(1,60)= 87.95 (metabolic condition, panel 3B) with p < 0.0001.

significantly reduced tumor cell growth by decreasing both neovascularization (CD31 + areas) and proliferative rate (Ki67 + areas). Notably, the results revealed not only the efficacy of the single cannabinoids, but also suggested that, when combined, CBD and CBG exert a promising anti-tumor action in vivo.

To further assess the potential of drug combination for in vivo treatment of PCa, we performed combination treatments on non-HRPC cells with increasing concentrations of both CBD and CBG to determine the potential combinatorial effect of these drugs (Fig. 7A). The drug combination responses were obtained using the ZIP reference model in SynergyFinder [23] and the results of such analysis are shown by the ZIP synergy score, where positive deviations between observed and expected responses imply synergy (in red), while negative values denote antagonism (in green). As it can be observed in Fig. 7A, results show an additive anti-tumor effect (in white) of the two drugs along the 1:1 ratio diagonal. Outside the 1:1 combination, areas of antagonism (in green) can be observed, thus supporting the effectiveness of a 1:1 combination treatment.

These results prompted us to perform additional experiments in vivo exploiting the multistage PCa model represented by the TRAMP mouse [16]. Animals were treated from the appearance of the early Prostatic Intraepithelial Neoplasia (PIN) phase (at the age of 12 weeks) up to 18 weeks of age, when well differentiate tumors are already developed. As shown in Fig. 7B and C, the histopathological quantification of transformed/pathological areas in the prostate lobes revealed that single (75 mg/kg) and combined (37.5 + 37.5 mg/kg) treatments with CBD and CBG significantly reduced tumor burden in terms of transformed areas, CBD and the combination CBD:CBG being the most effective at this stage of the disease.

The in vivo tolerability of these molecules was also evaluated (by treating C57BL/6 male mice for 6-weeks) and no relevant changes were detectable in terms of hematological and biochemical blood parameters in blood samples (Table S1). Only a slight increase in the number of White Blood Cells (WBC) and of ALT transaminase was found, mainly attributable to CBG, and this effect was much improved when the two drugs were administered in combination at lower concentrations.

In consideration of these results, and given that CBD and CBG induce PCa cell death on both non-HRPC and HRPC cells via different mechanisms of action, we tested the combination CBD:CBG in an in vivo therapeutic setting further mimicking the onset of hormone resistance

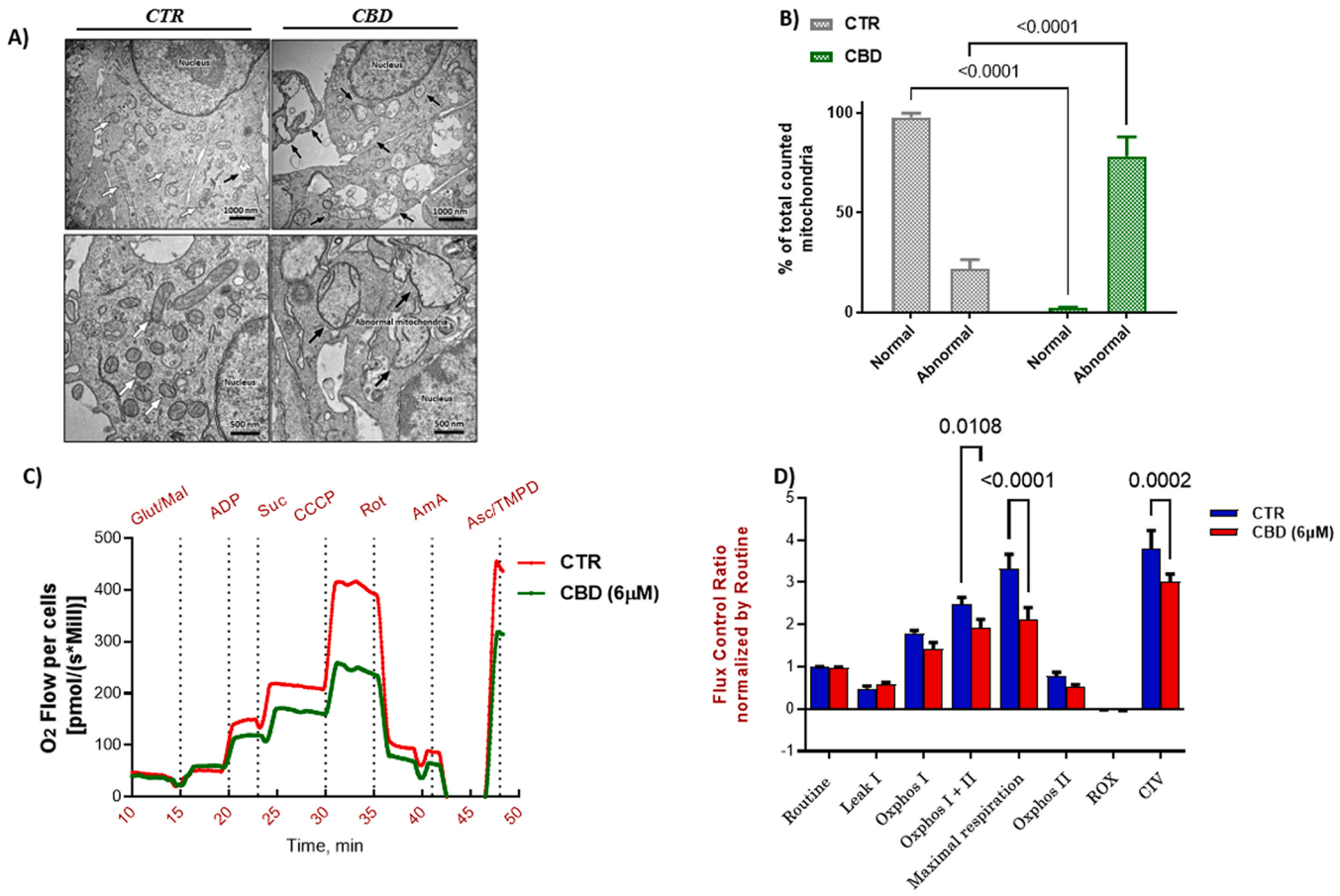

Fig. 4. CBD promotes cristae fragmentation and reduces maximal respiration capacity in HRPC cells. (**A**) Representative images acquired by Transmission Electron Microscopy using a TECNAI-12 electron microscope equipped with an ultra-view CCD digital camera (Philips, Eindhoven, The Netherlands). Normal mitochondria are indicated by white arrows, abnormal mitochondria are indicated by black arrows. (**B**) Quantification of mitochondrial morphology was performed as described using the AnalySIS software (Soft Imaging Systems GmbH, Munster, Germany). (**C**) Representative oxygen level tracing on digitonin-permeabilized HRPC cells (1 million) measured by O2K-FluoRespirometry according to SUIT protocol. (**D**) Mitochondrial respiration corrected for residual oxygen consumption (ROX) and for the different coupling/pathway control states. Normally distributed data are reported as mean ± SEM of independent experiments (n = 3 run in triplicate in panel 4B; n = 6 run in duplicate in panel 4D). For statistical analysis, two-way ANOVA followed by Sidak multiple comparison test was used with $F(1,8)= 574.1$ and 37.60 (interaction and treatment, respectively [panel 4D] with $p < 0.0001$); $F(7,40)= 7.687$ and 52.07 (Respiratory state per treatment and Respiratory state, respectively [panel 4D] with $p < 0.0001$); $F(1,40)= 45.77$ (treatment, panel 4D with $p < 0.0001$); $F(40,40)= 4.2141$ (time, panel 4D with $p < 0.0001$).

status by using TRAMP mice with acquired enzalutamide resistance [16]. To this purpose we performed combination treatments on enzalutamide-resistant HRPC cells with increasing concentrations of both CBD and CBG to determine the potential combinatorial effect of these drugs. As shown in Fig. 7D, the ZIP synergy score, strongly indicated for low concentrations of CBD and CBG a synergistic effect of the combination CBD:CBG in triggering cell death in HRPC conditions. A combination treatment with the three drugs (enzalutamide, CBD and CBG) was also tested showing clear synergy in the enzalutamide+CBG combination on HRPC cells (Fig. S14).

As previously shown in vivo [16], treatment with enzalutamide (3 mg/kg), staring from week 12 of age, restrains tumor growth till week 22 of age in TRAMP mice, when prostate tumors become resistant to treatment and relapses are observed, resulting in well differentiated PCa again at week 25. As shown in Fig. 8A, when the CBD:CBG combination (1:1) was evaluated in naïve TRAMP mice up to week 25 of age, a significant reduction of the pathological area was observed in the prostate of treated mice, and this effect was even stronger if compared with the enzalutamide only-treated group. In addition, concurrent and continuous treatment with CBD:CBG and enzalutamide (from week 12 to week 25) significantly reduced the hormone-refractory phase growth of TRAMP tumors, maintaining the disease at "starting levels" similar to the 12-week age group (see histopathological analysis in Fig. 8A and its quantification in Fig. 8B). We also explored the effect of the drug combination solely in the enzalutamide-resistant setting of the disease treating mice with CBD:CBG only from week 22 to week 25, when tumor growth has become refractory to treatment with enzalutamide (from week 12–22). Notably, also in this case the cannabinoids exerted a strong therapeutic effect significantly reducing the disease if compared with enzalutamide treatment alone till week 25 (Fig. 8A and B).

3. Discussion

CBD and CBG inhibit tumor growth in human PCa cells and xenograft models [11,24] although through different and not completely elucidated mechanisms. Currently, a phase I/Ib study is evaluating the safety and effectiveness of Epidiolex (CBD) in biochemically recurrent PCa patients (Clinical Trials Identifier: NCT04428203) [25]. From a metabolic perspective, PCa is a disease of great interest as, differently from other types of cancer, it follows the Warburg effect (*aka* the preferential metabolic shift from oxidative phosphorylation to enhanced conversion of glucose to lactate observed in cancer cells even in the presence of normoxic conditions) only in its high-grade phase [26]. Molecular links between metabolic stress and cell death are poorly understood [27]. However, the existence of such metabolic features in this HRPC phase supports their use as therapeutical targets and points out the need of

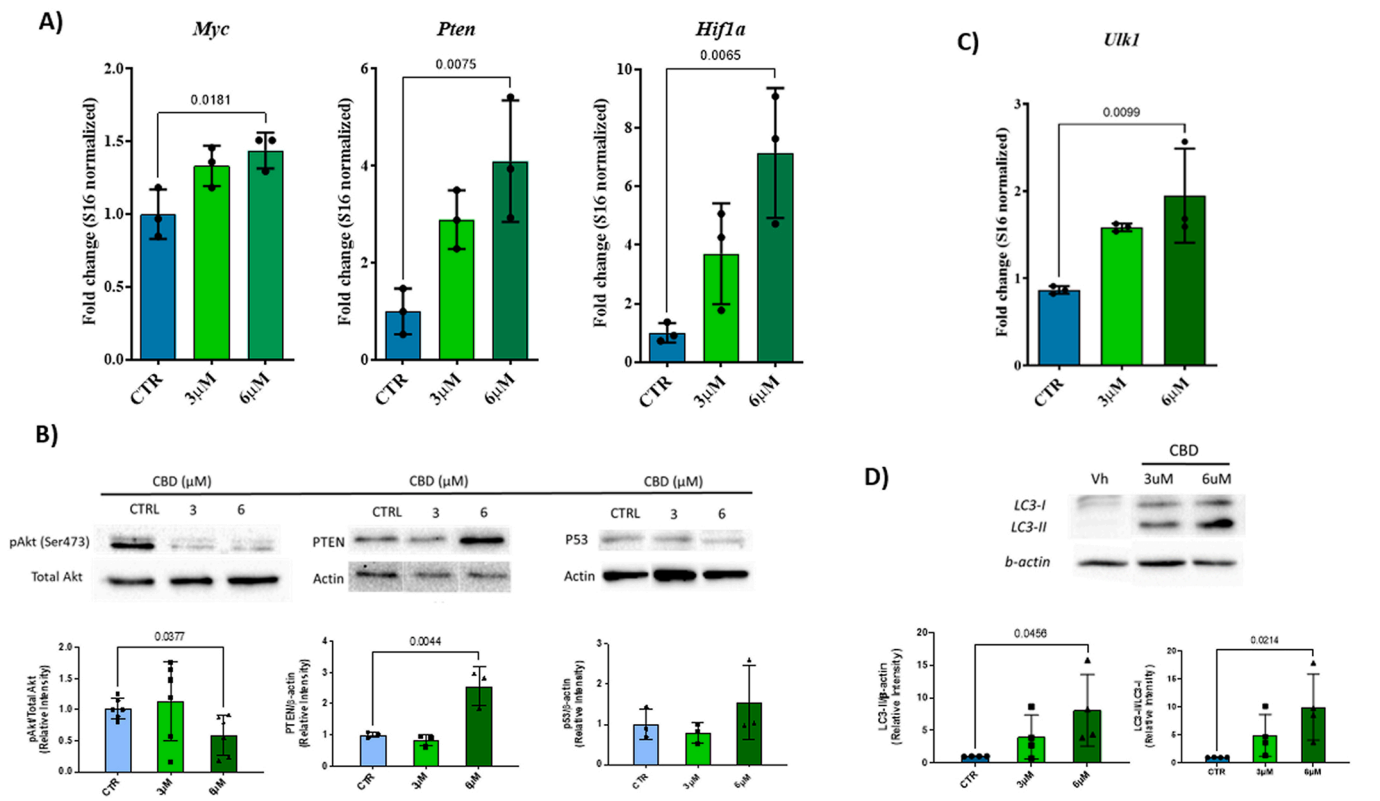

Fig. 5. CBD-mediated deregulation of cellular metabolism alters oncogenic signaling and transcription factors in HRPC cells. Real-time PCR gene expression analysis of selected targets (A and C). Western Blot analysis of PTEN, pAkt, LC3II in HRPC cells. Protein bands are reported together with corresponding quantification (B and D). Normally distributed data are presented as scatter plot bars indicating mean + SD of fold changed normalized by β-actin (panel 5B) and/or LC3I (panel 5D) of independent experiments (n = 3 in duplicate in ^{5}A–^{5}B-5 C, n = 4 in duplicate in 5D, n = 6 in duplicate in 5B [pAkt/totalAkt]). For statistical analysis, ordinary one-way ANOVA followed by Dunnet's was used with F(2,6)= 19.57 and 1.273 (PTEN and p53 in 5B, respectively); F(2,15)= 1.854 (pAkt/total Akt in 5B); F (2, 6)= 9.247 (in panel 5 C); F (2,9)= 3.601 and 4.977 (LC3-II/act and LC3-II/LC3-I, respectively in panel 5D).

further investigations validating the efficacy of molecules acting on both cell metabolism and cell death. Located at the outer mitochondria membrane, VDAC1 is a key player in cancer cell metabolic programming as it controls metabolism switching and cell death signaling depending on its oligomerization state and conductance. In its open and high conductance state, VDAC1 supports OXPHOS. In its closed state and low conductance, VDAC1 supports the Warburg effect by switching cancer cell metabolism. HK-II overexpression and binding to VDAC1 are reported to inhibit apoptosis and induce cell proliferation in cancer [28]. VDAC1-bound to HK-II was reported to maintain VDAC1 in open state leading to constant supply of ATP for HK-II [29] indicating that HK-II interaction with VDAC1 regulates channel selectivity and cell fate signaling. By its binding to VDAC1, CBD was shown to decrease VDAC1 conductance [20]. Overexpression and uncoupling of HK II from metabolism are reported to induce autophagy by the mTOR pathway [30]. In this study we suggest that, in HRPC cells, CBD might lock VDAC1, or confine it from binding to HK-II, thus resulting in the increase of "VDAC1-free" ratio of HK-II leading to apoptosis as well as higher glycolytic rate and autophagy as depicted in the cartoon scheme (Fig. 8C).

We report that, in TRAMP-C2 cells, CBD and CBG provoke apoptosis-induced cell death regardless of their sensitivity to enzalutamide or dependence on hormones. However, the activation of caspases was significantly greater in CBD-treated compared to CBG-treated cells, and enzalutamide-resistant HRPC cells were more sensitive than non-HRPC cells to the pro-apoptotic effect of cannabinoids. Considering the intimate link between cell death and the bioenergetics processes mediated by the remodeling of the mitochondrial ultra-structure during apoptosis, we investigated the effect of these cannabinoids on main metabolic pathways. NMR-based metabolomics revealed that in both naïve non-HRPC and HRPC cells CBD treatment induces different alterations with respect to CBG treatment. Particularly, in HRPC cells CBD treatment induced a preponderance of metabolites linked to glycolysis. Accordingly, and merely in HRPC cells, Seahorse analysis showed that only CBD produced significant increase of glycolytic capacity together with reduced maximal OXPHOS capacity. CBD-mediated mitochondria targeting in HRPC cells was indeed an early event already visible after 3-hour treatment. CBD was also found to induce a plethora of other events (i.e., reduction of membrane potential, induction of cristae fragmentation and fission, inhibition of both Complex I-II and Complex IV) that determine a massive mitochondrial dysfunction in these cells. The key target of CBD was VDAC1 channel since when we blocked CBD effect on this channel with DIDS, a VDAC1 oligomerization inhibitor, the effect on cell viability, caspases and mitochondrial ATP was significantly reduced. In addition, we found that after a 24-hour treatment, CBD down-regulated phosphorylated Akt protein levels. This is important, since activated Akt prevents closure of the PT pore component of VDAC1 by promoting its coupling to HK-II [31].

Overall, all these events mediated by CBD occurred at the mitochondrial level and altered the expression of relevant transcription factors (i.e., HIF-1α), oncogenic signaling (i.e., cMyc) and tumor suppressor protein like PTEN, whose deletion in PCa promotes metabolic reprogramming and fuels malignant growth and proliferation [32]. On the other hand, CBD induced a significative time-dependent mitochondrial recruitment of HK-II, which wrenches HRPC cells by accelerating glycolytic capacity and promoting autophagy. Accordingly, CBD increased ULK1 mRNA levels and LC3II protein contents in HRPC cells. This is a novel, yet undescribed action for in vitro CBD-mediated cell death, which provides a mechanistic explanation as to how CBD, by inducing mitochondrial perturbations, promotes a hypoxic environment

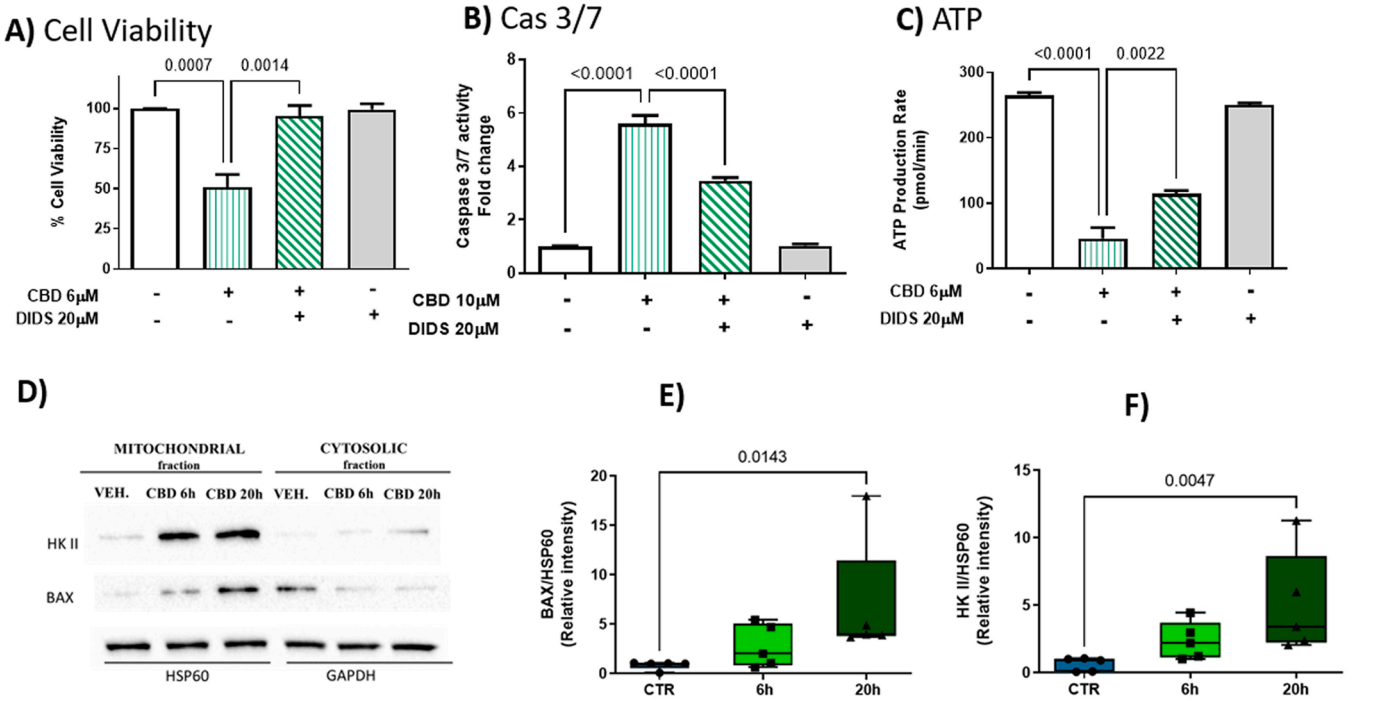

Fig. 6. CBD mitochondrial-induced actions are mediated by VDAC1 in HRPC cells. Effect of CBD in the presence and absence of DIDS on (A) cell viability by means of SRB assay, (B) caspase activation by means of CaspGlo assay and (C) mitochondrial ATP quantified by High Resolution Respirometry. Western Blot analysis of HK-II and BAX (D). Representative protein bands are reported together with the corresponding quantification (E-F). Normally distributed data are reported as mean ± SD of independent experiments (n = 3 in triplicate for 6 A and 6 C, n = 4 in quadruplicate for 6B). Not-normally distributed data are reported as scattered dot plot indicating median + IQR of relative intensity (n = 5 in duplicate for 6E and 6 F). For statistical analysis, ordinary one-way ANOVA followed by Sidak's (^{6}A–^{6}B-6 C) or Kruskal-Wallis followed by Dunn's (6E and 6 F) multiple comparisons test was used with F(3,8)= 18.64, 163.4 and 136.1 (6 A, 6B and 6 C, respectively) and K-W statistic: 7.293 (p value 0.0172) and 9.620 (p value 0.0018) (6E and 6 F, respectively).

that alters the metabolic adaptations of HRPC cells and induce their death.

Interestingly, in vivo, cannabinoids exerted efficient therapeutic effects on PCa both per se and in combination. This was not surprising, given that, in PCa, different cell types exist and emerge during tumor growth and evolution, in response to therapeutic approaches, and in view of the different mechanisms of action of CBD and CBG on naïve/non-HRPC and HRPC cells in vitro. Indeed, the combination of these drugs produced a striking effect also when combined with enzalutamide, and, in agreement with our in vitro studies, also in TRAMP mice that had become refractory to enzalutamide, paving the way for the evaluation of combination regimens aimed at preventing the long-term occurrence of the hormone-refractory PCa.

In conclusion, the present findings suggest a role for VDAC1-HKII coupling in HRPC cell metabolic plasticity supporting the existence of metabolic and oncogenic targetable vulnerabilities in HRPC that can potentially be therapeutically exploited by phytocannabinoid-based treatments. In particular, we showed how the capability of CBD to bind to VDAC1 and modify its interaction with HK-II leads to metabolic reprogramming resulting in apoptosis and autophagy of HRPCs, thus possibly explaining why this compound, alone or in combination with CBG, can significantly ameliorate the sensitivity of hormone-refractory TRAMP mice to the standard-of-care androgen targeting drug, enzalutamide. These findings should foster future studies, including clinical trials, on the possible use of botanical non-psychotropic cannabinoids as adjuncts for PCa treatment.

4. Materials and methods

4.1. Materials

Authors were provided once per year with a new batch of pure CBD and CBG extracts (purity ≥98%) by GW Pharmaceuticals. AL holds a formal good standing authorization (SP/72 prot. 0049640–09/07/2021-DGDMF-MDS-P) to manage controlled substances for research purpose in accordance with the Ministry of Health Directives.

4.2. Cell culture

TRAMP-C2 cell line was obtained from ATCC-LGC Standards Repository (ATCC number CRL-2731) and maintained in DMEM supplemented with 10% heat inactivated fetal calf serum (FCS), 10 mM HEPES Buffer, 0.5 mM 2-mercaptoethanol (as reducing agent to maintain the proteins activity), 2.0 mM glutamine, 5 mg/L bovine insulin (Sigma-Aldrich) and 10 nM DHT. Hormone-refractory TRAMP-C2 cells were generated as previously reported (REF). Only cells from passage N° 40 to passage N° 80 were used for the experiments.

4.3. Cell count assay

TRAMP-C2 cells were seeded in 96-well plates at 1×10^4 cells/well and treated with enzalutamide or cannabinoids (CBD and CBG). Cells were cultured under appropriate conditions. Propidium iodide staining (Immunostep, Salamanca, SP, EU) was used to detect PI-viable cells by flow cytometry. Cells were washed in PBS, resuspended in PBS containing 0.5% EDTA (Sigma Aldrich) and fixed in 99% ethanol for 12 h at 4 °C. Then cells were stained for 3 h at 4 °C with PBS containing 2% FBS, 12.5 μg/ml DNase-free RNase A (Sigma Aldrich) and 40 μg/ml of propidium iodide (Sigma Aldrich). Absolute cell counts were obtained by the counting function of the MACSQuant Analyzer (Miltenyi Biotec). Data are shown as mean ± SEM of 3 independent experiments run in duplicate.

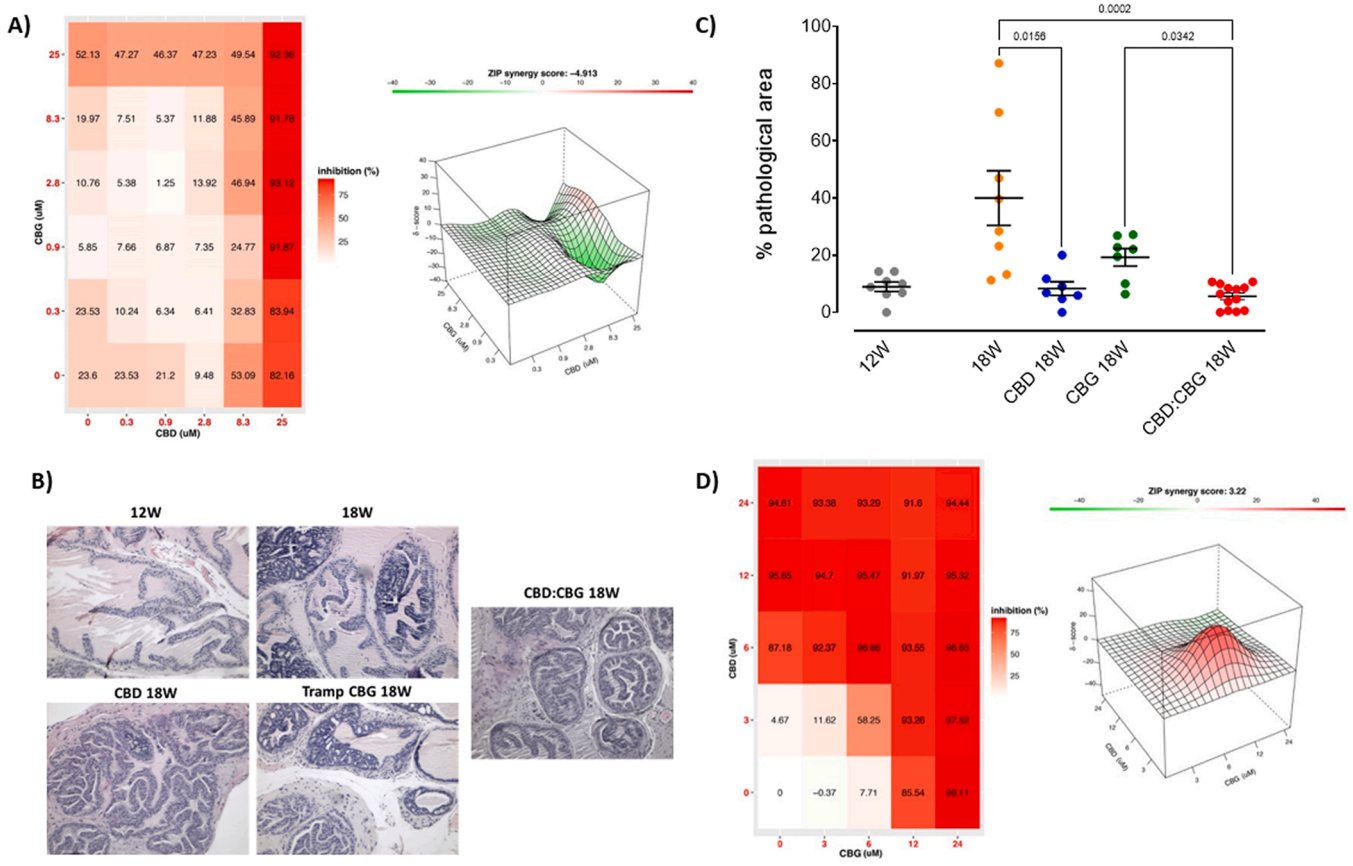

Fig. 7. Effect of CBD and CBG on tumor growth. Cell proliferation assay was performed on non-HRPC (**A**) and HRPC (**D**) cells to test the combination of CBD and CBG at different concentrations. Dose-response matrices and 3D synergy landscape plots are shown (**A**, **D**). Positive deviations between observed and expected responses imply synergy (in red), while negative values denote antagonism (in green). Effect of single (75 mg/kg) and combined (37.5 +37.5 mg/kg) treatments with CBD and CBG on the percentage of pathological area in TRAMP mice i.p. treated for 6 weeks twice per week from week 12 up to week 18 together with representative picture (H&E staining) of anterior prostate lobes are shown (**B, C**). Non-normally distributed data are reported as scatter dot plot indicating median + IQR of histopathological acquisitions (n = 8 mice for 12 W and 18 W; n = 7 mice for CBD and CBG; n = 13 mice for CBD:CBG) and analyzed using Kruskal-Wallis followed by Dunn's post hoc (K-W statistic 23.08 with p = 0.0001).

4.4. Cell viability colorimetric assay

Exponentially growing cells were collected using 0.25% Trypsin-EDTA and plated in 96-well plates at 1×10^4 cells/well. Cells were exposed to each treatment for 24 h in 0.4% FBS then fixed with TCA (10%) for 1 h at 4°C. After several washings, cells were exposed to 0.4% Sulforhodamine B (SRB) solution for 10 min in dark place and subsequently washed with 1% glacial acetic acid. After drying overnight, Tris-HCl was used to dissolve the SRB-stained cells and color intensity was measured was read on a GloMax® Explorer system (Promega, Milan, Italy) at 540 nm. Data are shown as mean ± SEM of at least 3 independent experiments run in triplicate.

4.5. Measurement of caspase 3/7 activity

Apoptosis was evaluated by means of the Caspase-Glo® 3/7 Chemiluminescent Assay Kit (Promega Corporation, Madison, WI, USA) following the manufacturer's protocol. Cells were cultured in the presence of CBD with 1, 10, and 30 μM for 3 h. After incubation, cells were trypsinized, washed with PBS and processed. The assay was performed in 96-well white-walled plates, adding 100 μl of Caspase-Glo® 3/7 reagent to each well with 100 μl of culture medium with cells. After 1 h incubation in the dark at room temperature, luminescence was measured by GloMax® Explorer system (Promega, Milan, Italy). Data are shown as mean ± SEM of at least 3 independent experiments run in triplicate.

4.6. RNA purification and quantitative RT-PCR analyses

Total RNA was extracted from cell pellets in 1.0 ml of Trizol® (Invitrogen) following the manufacturer's instructions, dissolved in adequate volume of RNA-DNA free water. RNA aliquots were digested by RNase-free DNase I (Invitrogen) in a 10 μl final volume reaction mixture to remove residual contaminating genomic DNA. After DNase digestion, RNA integrity has been tested by running the samples on agarose gel. Concentration and purity of RNA samples were evaluated by UV-quantified by a Bio-Photometer® (Eppendorf, Hamburg, Germany) following the manufacturer's instructions and stored at − 80 °C until Use. 1 μg of total RNA was reverse-transcribed in cDNA (Invitrogen, SuperScript™ III). qPCR was done using SYBR green master mix in CFX384 Real Time detection system (Bio-Rad™) Relative gene expression calculation, corrected for PCR efficiency and normalized with respect to the reference gene, was performed by the Bio-Rad CFX™ manager software.

4.7. Western blot analysis

Cells were washed two times in cold PBS (without Ca2 + and Mg2 +, pH7.4), then cells were lysed with lysis solution (150 mM NaCl, 1 mM EDTA, pH 7.4, 10 mM Tris-HCl pH 8, 1% SDS and 1% protease inhibitors). After the homogenization, cells have been centrifuged for 15 min at 13,000g at 4 °C. Protein concentrations were determined using the Bradford protein assay (Bio-Rad Laboratories, Milano, Italy).

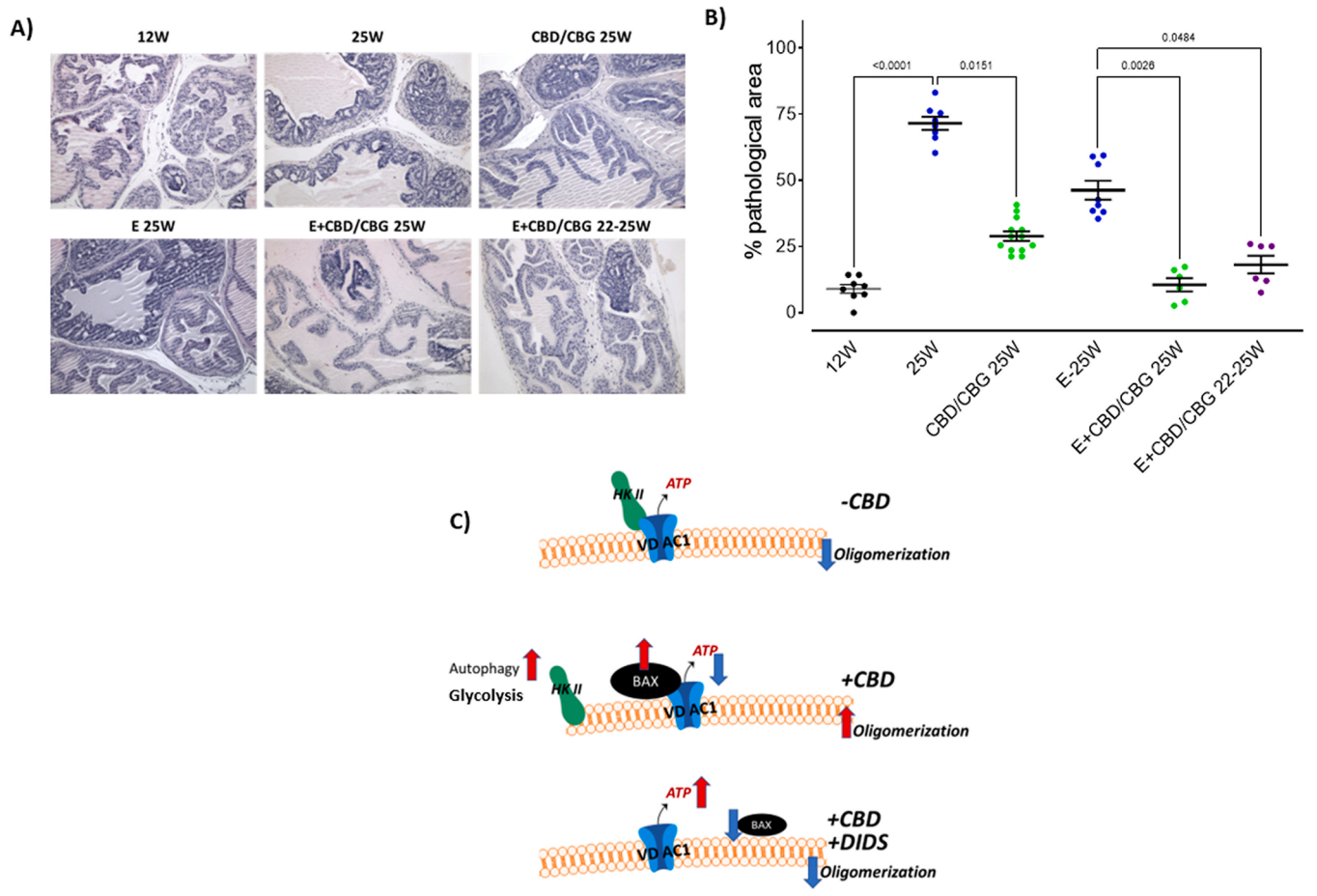

Fig. 8. CBD and CBG in combination reduce enzalutamide-resistant tumor growth in vivo.
Effect of CBD:CBG on the percentage of pathological area in TRAMP mice treated for 13 weeks (twice per week from week 12 up to week 25) with a 1:1 combination CBD:CBG (37.5 +37.5 mg/kg) is reported together with representative picture (H&E staining) of anterior prostate lobes (**A**, **B**). Non-normally distributed data are reported as scatter dot plot indicating median + IQR of histopathological acquisition (n = 6 for E + CBD:CBG 25 W and E + CBD:CBG 22–25 W; n = 8 for 12 W 25 W and E-25 W; n = 13 for CBD:CBG 25 W) and analyzed using Kruskal-Wallis followed by Dunn's post hoc test (K-W statistic 41.87 with $p < 0.0001$). A schematic representation of the possible mechanism of action of CBD at mitochondrial level is also reported (**C**).

Blotting analysis was performed using anti-phospho Akt and total Akt antibodies (Cell Signaling), FIS1 (BioVision), MFN1 (H-65) (Santa Cruz Biotechnology), PTEN (Cell Signaling), LC3B (Cell Signaling), B-actin (Cell Signaling), P53 (Cell Signaling), Hexokinase II (Cell Signaling), BAX (B-9) (Santa Cruz Biotechnology), HSP60 (H-300) (Santa Cruz Biotechnology), GAPDH (Novus Bioloigicals).

4.8. NMR spectra acquisition

Cells were seeded (1 million per dish, n = 5/experimental group) one day before harvesting in 10 cm Petri dishes and treated with CBD or CBG (3 and 6 μM) for 24 h. After incubation, cells were harvested on ice and stored at − 80 °C until metabolites extraction. NMR spectra were recorded at 600.13 MHz on a Bruker Avance-600 spectrometer, equipped with a TCI CryoProbe™ fitted with a gradient along the Z-axis, at a probe temperature of 27 °C. 1D proton spectra of cells were acquired using the excitation sculpting sequence. A double-pulsed field gradient echo was used, with a soft square pulse of 4 ms at the water resonance frequency, with the gradient pulses of 1 ms each in duration, adding 256 transients of 16,384 points with a spectral width of 8389.3 Hz. Time-domain data were all zero-filled to 32,768 points, and prior to Fourier transformation, an exponential multiplication of 0.6 Hz was applied. Two-dimensional (2D) experiments were recorded to assist signal identification of discriminant metabolites. To that purpose, clean total correlation spectroscopy (TOCSY) spectra were recorded using a standard pulse sequence and incorporating the excitation sculpting sequence for water suppression. In general, 320 equally spaced evolution-time period t1 values were acquired, averaging 4 transient of 2048 points, with 7002.8 Hz of spectral width. Time-domain data matrices were all zero-filled to 4096 points in both dimensions, thus yielding a digital resolution of 3.42 Hz/pt. Prior to Fourier transformation, a Lorentz-to-Gauss window with different parameters was applied for both t1 and t2 dimensions for all the experiments. TOCSY experiments were recorded with spin-lock period of 64 ms, achieved with the MLEV-17 pulse sequence. Spectra were referred to 0.1 mM sodium trimethylsilylpropionate (TSP), assumed to resonate at δ = 0.00 ppm. In addition, natural abundance 2D 1 H–13 C heteronuclear single quantum coherence (HSQC) spectra were recorded at 150.90 MHz for 13 C, using an echo–antiecho phase sensitive pulse sequence with adiabatic pulses for decoupling and water suppression using pre-saturation. 128 equally spaced evolution time period t1 values were acquired, averaging 240 transient of 2048 points and using GARP4 for decoupling. The final data matrix was zero–filled to 4096 in both dimensions, and apodised before Fourier transformation by a shifted cosine window function in t2 and in t1. Linear prediction was also applied to extend the data to twice its length in t1. HSQC spectra are referred to the lactate doublet (βCH3) resonating at 1.33 ppm for 1 H and 20.76 ppm for 13 C.

4.9. NMR data analysis

The 0.60–9.60 ppm proton region of cell spectra was automatically data reduced to 450 integrated regions (buckets) of 0.02 ppm width using the AMIX 3.9.7 package (Bruker Biospin GmbH, Rheinstetten, Germany). The residual water resonance region (5.16–4.50 ppm) was excluded, and each integrated region was normalized to the total spectrum area to avoid possible signal variation due to dilution of samples, which could result in an artificial increase of the signals. To discriminate the different class of samples through NMR spectra according to the condition/treatment of mice, we carried out a multivariate statistical data analysis using projection methods. The integrated data reduced format of the spectra was imported into SIMCA 14 package (Umetrics, Umeå, Sweden), and Principal Component Analysis (PCA) and Orthogonal Partial Least Squares Discriminant Analysis (OPLS–DA) were performed. Mean–centering and Pareto scaling were used as data pre–treatment for both PCA and OPLS–DA. PCA was first applied to extract and display the systematic variation in the data matrix so to identify trends and clustering in an unsupervised manner. However, to better define grouping and select molecular markers related to specific experimental treatments/conditions, supervised OPLS–DA analysis was used. Metabolite Set Enrichment Analysis (MSEA) to identify biologically meaningful patterns that are significantly enriched in selected and more representative metabolites in class separation was applied to the pathway topology search tool in Metaboanalyst 4.0. In this analysis, the metabolic "pathway-associated metabolite sets" (currently containing 88 entries) from human library was selected. Over Representation Analysis was implemented using the hypergeometric test to evaluate whether a particular metabolite set is represented more than expected by chance within the selected compound list. Metabolites were selected by evaluating both VIP values > 1 in class discrimination and correlation values $|p(corr)| > 0.7$.

4.10. Measurement of extracellular acidification rates (ECAR) and oxygen consumption rate (OCR)

ECAR and OCR measurements were conducted using the XF96 Extracellular Flux analyzer (Seahorse Bioscience). Briefly, cells were seeded at 4×10^5/well in XF96 cell culture plates and were incubated for 24 in a humidified 37 °C incubator with 5% CO2. Before starting, growth medium was replaced with appropriate assay medium. All experiments were performed at 37 °C. Each measurement cycle consisted of a mixing time. ECAR and OCR data points referred to the average rates during the measurement cycles. All compounds were prepared at appropriate concentrations in desired assay medium and adjusted to pH 7.4. In a typical experiment, 3 baseline measurements were taken prior to the addition of any compound, and 3 response measurements were taken after the addition of each compound. ECAR and OCR were reported as absolute rates (mpH/min for ECAR and pmoles/min for OCR) [33].

4.11. MitoSOX-based flow cytometric detection of mitochondrial ROS

Cells were seeded (1×10^4 cells/well), treated with different concentrations (3 and 6 μM) of CBD for 24 h, and harvested by trypsinization. MitoSOX™ Red Mitochondrial Superoxide Indicator (Molecular Probes™) was used as a probe for mtROS at 1 μM for 20 min at 37 °C with shaking. Cells were then washed and centrifuged. Cell pellet was resuspended with PBS solution containing 8.1 mM Na2HPO4, 1.47 mM KH2PO4, 138 mM NaCl, 2.67 mM KCl, 0.5 mM MgCl2, 0.7 mM CaCl2, and 0.1% glucose, pH 7.4, for FACS analysis. Experiments were performed in triplicate.

4.12. Mitochondrial ROS measurement by O2K-FluoRespirometer analysis

The Oxygraph-2k (O2k, OROBOROS Instruments, Innsbruck, Austria) combined with the Fluorescence-Sensor Green of the O2k-Fluo LED2-Module was used to assess H2O2 measurement in permeabilized cells. Experiments were performed in MiR05 (110 mM sucrose, 60 mM K-lactobionate, 0.5 mM EGTA, 3 mM MgCl2, 20 mM taurine, 10 mM KH2PO4, 20 mM HEPES, pH 7.1 at 30 °C, and 0.1% BSA essentially fatty acid free). The medium was reoxygenated when oxygen concentrations fell to 80 μM unless otherwise indicated. Samples were run in parallel by using two chambers per time (untreated-cells versus treated-cells).

4.13. Agilent Seahorse XF real-time ATP rate assay

Cells were assessed using the Agilent Seahorse XF real-time ATP rate assay kit on a Seahorse XFe96 extracellular flux analyzer, according to the manufacturer's instruction. Cells were seeded (1×104 cells/well) and treated with CBD (3 and 6 μM for 24 h), then washed with 200 μl of a 1X warm ATP Assay Medium. Cells were incubated at 37 °C for 45 min, medium was removed and replaced with 200 μl of fresh ATP Assay medium. Finally, cells were measured using the Seahorse XFe96 Extracellular Flux. Data were analyzed in the Agilent ATP Assay Report Generator and statistics were analyzed by Prism software.

4.14. Mitochondrial ATP production/respiration rate measurement by O2K-FluoRespirometer analysis

The ATP production rate was obtained by O2K Oroboros instrument as an indirect measurement from the oxygen consumption rate (OCR) calculated according to the SUIT (substrate-uncoupler-inhibitor titration) protocol, which was optimized for measuring ATP production rate by our lab. SUIT protocol has been followed by the addition of 8.1 μM Digitonin; 5 mM Pyruvate, 10 mM Glutamate and 2 mM Malate, Succinate 10 mM (substrates of complex I + II), then Oligomycin (~2 μM) to inhibit complex V, then 0.5 μM rotenone (Rot) plus 2.5 μM antimycin A (AmA) to calculate the ROX. The OCR coupled with ATP production was calculated as the difference in the OCR values before and after the addition of Oligomycin (Complex V inhibitor) to consider only the inhibition of OCR. To measure the ATP molecules generated, this "normalized" OCR value was first multiplied by 2 to calculate oxygen atoms (O) and further was multiplied by the P/O value (the conversion to ATP phosphorylated form from atoms of oxygen reduced), which is around 2.75. By applying this procedure, ATP production rate as the amount of ATP molecules produced by complex V from mitochondria was calculated.

4.15. Analysis of the inner mitochondrial membrane potential ($\Delta\Psi m$)

Cells were seeded (7×10^4 cells/well) in 24 well-multiwell plates and 24 h later were treated with different concentrations of GWP42003 (0.1 μM, 3 μM and 6 μM) for 24 h. Cells were treated with TMRM (Invitrogen) dye (50 nM) for 30 min before they were trypsinized, resuspended in the growth medium and transferred to the flow cytometer (Gallios; Becton Dickinson). Data were acquired and analyzed by using the BD CellQuest™Pro Software (BD Biosciences). Fluorescence values were determined on 5000 cells for each condition in each experiment. Values were normalized by mitochondrial mass values in each experiment, and for each condition. CCCP treatment (100 μM) 30 min prior to the TMRM treatment was used as negative control for each experimental condition analyzed.

4.16. Mitochondrial mass assessment by FACS

Cells were seeded (7×10^4 cells/well) in 24 well-multiwell and the

day after were treated with different concentrations of GWP42003 (3 μM and 6 μM) for 24 h. Cells were treated with mito-tracker green dye (50 nM) for 30 min before they were trypsinized, resuspended in the growth medium and transferred to the flow cytometer (Gallios; Becton Dickinson). Data were acquired and analyzed by using the BD Cell-Quest™Pro Software (BD Biosciences). Fluorescence values were determined on 5000 cells for each condition in each experiment.

4.17. Mitochondrial morphology assessment by microscopy

4.17.1. Super-resolution confocal microscopy

Cells were seeded (5 ×104 cells/well) in lab-tech chambers and, after adhesion, were treated with two concentrations of GWP42003 (3 and 6 μM) for 24 h. Cells were treated with mito-tracker green dye (50 nM) for 30 min before image acquisition over a range of multiple z-planes (minimum 4) by ZEISS Elyra Microscope.

4.17.2. Electron microscopy

Cells were fixed with 1% glutaraldehyde prepared in 0.2 M HEPES (pH-7.3) for 30 min at RT. Then the cells were washed, post-fixed with a 1% glutaraldehyde and 0.2 M HEPES. After dehydration the specimens were embedded in epoxy resin and polymerized at 60 °C for 72 hr. Thin 60 nm sections were cut at the Leica EM UC7 microtome. Electron micrograph images were acquired from thin sections using a FEI Tecnai-12 electron microscope equipped with a VELETTA CCD digital camera (FEI, Eindhoven, The Netherlands). To count the number and measure the size of mitochondria the iTEM software (Olympus SYS, Germany) was used. The structures (phenotypes) present on representative images were analyzed. Over 200 mitochondrial structures per sample were analyzed (10–15 micrographs that correspond to the representative cell/field and allowed to perform such analysis). To run sample analysis, an external operator went through all the material present on the 60 nm thick section placed on 200 mesh grid. Each section occupied 10 or 30 squares (mesh) in order to find 6–10 cells per 1 mesh. Sample size analysis varied from 60 cells (10 squares x 6 cells) - 300 cells (30 squared x 10 cells).

4.18. Analysis of mitochondrial respiratory parameters by O2K-FluoRespirometer (Oroboros)

Experiments were performed on permeabilized cells trypsinized, centrifuged and resuspended in respiration buffer to a final density of 1×10^6 cells/ml. To calibrate the Oroboros chamber's electrode, respiration buffer was pipetted into an oxygraph chamber and continuously stirred for 1 h until a stable oxygen flux signal of the polarographic oxygen sensor was obtained. Air calibration of the polarographic oxygen sensor was performed according to the manufacturer's protocols. For High-resolution respirometry, after air calibration, respiration medium was removed, and cell suspension was placed into the oxygraph chamber under continuous stirring to record cellular respiration (5–10 min) until a stable oxygen flux signal was achieved. Appropriate substrates and inhibitors for mitochondrial respiration were added through the titanium injection ports. Cells were resuspended in the respiratory media applied directly to the Oroboros. Intact cells were instead treated to increase their cell permeability, 2 μl of 2 mM permeability agent solution (digitonin) were injected into the oxygraph chamber and cellular respiration was recorded until a stable oxygen flux signal was achieved. After this step, 12.5 μl of 0.8 M of malate (5 mM) and 10 μl of 2 M of glutamate (10 mM) were injected into the oxygraph chamber and cellular respiration was recorded until a stable oxygen flux signal was achieved measuring leak I respiration. Afterwards, 20 μl of 1 M succinate (10 mM) were injected into the oxygraph chamber and cellular respiration was recorded until the oxygen flux signal increased and stabilized measuring leak I & II respiration. Further, 10 μl of 0.5 M ADP (2.5 mM) were injected into the oxygraph chamber and cellular respiration were injected until the oxygen flux signal increased and stabilized measuring OXPHOS I & II respiration). Then 2 μl of 0.2 mM rotenone (0.2 μM) were injected into the oxygraph chamber and cellular respiration recorded until the oxygen flux signal decreases and stabilized measuring OXPHOS II respiration. Then, 2 μl of 5 mM antimycin A (5 μM) were injected into the oxygraph chamber and cellular respiration recorded until the oxygen flux signal decreases and stabilized measuring residual oxygen consumption. Finally, 2.5 μl of 0.8 mM ascorbate (1 mM) followed by 2.5 μl of 0.2 mM TMPD (0.25 mM) were injected into the oxygraph chamber and cellular respiration recorded until the oxygen flux signal increases and stabilized. For measuring maximum capacity of oxygen consumption of intact cells using the Seahorse assay, 1 μl of 4 mg/ml oligomycin (2 μg/ml) were injected into the oxygraph chamber containing cell suspension and change in cellular respiration from baseline recorded until a stable oxygen flux signal is achieved enabling the measurement of ATP production and proton leak. Afterwards, 1 μl of 0.2 mM of FCCP (0.1 μM) were injected into the oxygraph chamber and cellular respiration recorded until the oxygen flux signal increases and stabilizes. Further, 3 μl of 0.2 mM of FCCP (0.4 μM) were injected into the oxygraph chamber and cellular respiration recorded until the oxygen flux signal increases further and stabilized measuring maximal respiration. Finally, 2 μl of 0.2 mM rotenone (0.2 μM) and 2 μl of 5 mM antimycin A (5 μM) were injected into the chamber and cellular respiration recorded until the oxygen flux signal decreases and stabilized measuring spare respiratory capacity. Different injection strategies were performed to measure all the other different mitochondria states and parameters.

4.19. Short term alginate plug assay

TRAMP-C2 murine prostate carcinoma cells (3×10^6) were injected s.c. into the flank of 7-week-old C56BL/6 male mice in 100 μl of PBS and 150 μl of 3% alginate. After 2 weeks, mice were treated i.p. with 200 μl of Vehicle [Ethanol/cremophor/saline (2:1:17)] containing single (75 mg/kg) or combined (37.5 + 37.5 mg/kg) dose of the two cannabinoids CBD and CBG. Treatments were performed every other day for one week. The day after the last treatment, mice were euthanized, and the pellets harvested for immunofluorescence analyses.

4.20. Immunofluorescence analysis of alginate plugs

For immunofluorescence analysis, alginate gels were embedded in OCT-compound and immediately frozen. Section (5 μm thick) were obtained with a cryostat microtome, air dried and fixed with acetone (for 5 min at 4 °C). After blocking with 1% BSA in PBS for 10 min, sections were incubated for 1 h at room temperature rat anti-mouse CD31 (BD Pharmingen) or rat anti-mouse Ki67 (Dako) primary antibodies. After washing with PBS containing 0.05% Tween 20, sections were incubated with the appropriate Alexa Fluor 488 or Alexa Fluor 594-conjugated secondary antibody (Invitrogen). After mounting in a drop of anti-bleaching mounting medium containing DAPI (Vectashield, Vector Laboratories, Burlingame, CA, USA), sections were examined under a Zeiss fluorescence microscope (Zeiss Inc., North America) equipped with an Olympus N547 digital camera (Olympus, Hamburg, Germany). Immunohistochemical quantitative assessment was performed by two examiners, blinded to experimental conditions. Sections were cut from paraffin-embedded tissues and routine sections were stained with hematoxylin and eosin stain for histological assessment and for immunohistochemical analysis. Evaluation of distribution of single or multiple immunostainings and of the relative optical density were quantified by application of deconvolution with Leica-MetaMorph LASAF2.2.0 software.

4.21. In vivo treatment of TRAMP mice

Initially, TRAMP mice (C57BL/6-Tg (TRAMP)8247Ng/J) were purchased from The Jackson Laboratory (Bar Harbor, ME, USA), then bred

crossing homozygous females with C57BL/6 J wild type males and heterozygous TRAMP males were used for experimental procedures. Experiments were carried out in Animal Facility at the University of Brescia and approved by the local animal ethics committee (OPBA, Organismo Preposto al Benessere degli Animali, Universita degli Studi di Brescia, Italy) as well as performed following national guidelines and regulations. Animals were housed under controlled temperature and standard 12 h/12 h light/dark cycle with food and water available ad libitum. Treatment was carried out adding enzalutamide (ENZA, MDV3100; Selleckchem), 3 mg/kg in the drinking water. Cannabinoids, kindly provided by GW Research Ltd (Cambridge, UK), were always administrated intraperitoneally (i.p), twice per week at the dose of 75 mg/kg when injected as pure (>99% w/w botanical compounds (CBD or CBG) and at half of their dose when injected as 1:1 combination CBD:CBG (37.5 +37.5 mg/kg) prepared in ethanol/cremophor/saline [2:1:17]. According to the FDA allometric scaling guidelines, 75 mg/kg in mice are equivalent to 6.075 mg/kg in human (REFS) which is a dose reported to be well tolerated in humans in the context of CBD. Treated or untreated mice were sacrificed at different time points, as indicated in the results section, to collect the genitourinary apparatus that was weighted and prepared for histology as described in Cerasuolo M. et al. and Chiodelli P. et al. [34].

4.22. Murine prostate histopathological analysis

The genitourinary apparatus was removed from wild-type or TRAMP male mice at different ages, formalin- fixed and paraffin-embedded. Anterior prostate samples were sectioned at a thickness of 7 μm, dewaxed, hydrated, and stained with hematoxylin and eosin (H&E) or processed for immunohistochemistry. Sections stained with H&E were evaluated for specific histological abnormalities. The full prostate section was acquired at 20x magnification with a Zeiss Axiovert 200 M microscope (Carl Zeiss, Milan, Italy, EU) using the "Mosaic Tool" and the quantification of the pathological areas was performed with the AxioVision LE64 software. Also, the number of pathological adenomeres was determined and pathological areas were graded as described [35].

For the immunohistochemical analysis, prostate sections were incubated with rat anti-mouse Ki67 antibodies (Dako, Milano, Italy, EU). Positive signal was revealed by 3,3′-diaminibenzidine (Roche) staining. Sections were finally counterstained with Mayer's hematoxylin before analysis by light microscopy. Images were acquired at 10x magnification with a Zeiss Axiovert 200 M microscope and Image analysis was carried out using the ImagePro Plus software.

4.23. Statistical analyses

Normal distribution was tested with the following tests: Shapiro-Wilk. For not-normally distributed data, the Kruskal-Wallis test was performed. For normally distributed data, one way or two-way ANOVA analyses were used. Dunnet's or Dunn's posthoc tests were applied after a one-way ANOVA to compare all groups vs vehicle. Sidak's posthoc test was applied for instances where there were pre-planned comparisons of interest. Sidak's or Tukey's were applied after a 2-way ANOVA for pre-planned comparisons of interest or for multiple comparisons of all groups, respectively. T test with Welch's correction was used to make comparisons between two groups and to evaluate whether fold changes are different from one, respectively. The analyses were performed using GraphPad version 9.3 for Windows, GraphPad Software, La Jolla, CA, USA.

CRediT authorship contribution statement

AL, **AMM**, **RR**: Study conception and design. **AMM, MK**, **VM**, **FM, DC, SR, AG, MPM, DP**: Data acquisition. **AL, RR, MC, AMM, DC, AM, AZ**: Data analysis/interpretation. **AMM, AL**: Manuscript drafting. **AL, RR, MC, AZ, VDM**: Critical manuscript revision for intellectual content.

Conflict of interest

The authors have no conflicts of interest to declare. All co-authors have seen and agree with the contents of the manuscript and there is no financial interest to report.

Data availability

Data will be made available on request.

Acknowledgments

The authors thank Jazz Pharmaceuticals, Inc. for funding this study. A.M.M. and M.K. were recipients of a scholarship from INCIPIT PhD program co-funded by the COFUND scheme Marie Skłodowska-Curie Actions (Grant Number 665403). A.M.M. was the recipient of a travel grant from the Unité Mixte Internationale en Recherche Chimique et Biomoléculaire du Microbiome et son Impact sur la Santé Métabolique et la Nutrition, which in turn was supported by the Federal Tri-Agency through the Canada First-Apogée programme and the Sentinel North fund. FM was supported by Fondazione Umberto Veronesi Felloship. Authors thank Dr. Raffaele De Palma for technical assistance with Seahorse experiments and Dr. Fabiana Piscitelli for technical assistance with LC-MS analysis. The images shown in Fig. 4 were acquired using Telethon Electron Microscopy Core Facility. CBD and CBG were provided by GW Research Ltd. A.L. was recipient of a research grant from GW Research Ltd and R.R. was supported by Associazione Italiana per la Ricerca sul Cancro (AIRC IG 2019 – ID. 23151).

Appendix A. Supporting information

Supplementary data associated with this article can be found in the online version at doi:10.1016/j.phrs.2023.106683.

References

[1] R.L. Siegel, K.D. Miller, A. Jemal, Cancer statistics, 2020, CA Cancer J. Clin. 70 (2020) 7–30.
[2] R. Schrecengost, K.E. Knudsen, Molecular pathogenesis and progression of prostate cancer, Semin. Oncol. 40 (2013) 244–258.
[3] R. Narayanan, Therapeutic targeting of the androgen receptor (AR) and AR variants in prostate cancer, Asian J. Urol. 7 (2020) 271–283.
[4] M.Y. Teo, D.E. Rathkopf, P. Kantoff, Treatment of advanced prostate cancer, Annu. Rev. Med. 70 (2019) 479–499.
[5] S. Linder, H.G. van der Poel, A.M. Bergman, W. Zwart, S. Prekovic, Enzalutamide therapy for advanced prostate cancer: efficacy, resistance and beyond, Endocr. Relat. Cancer 26 (2018) R31–R52.
[6] Y. Cui, et al., Upregulation of glucose metabolism by NF-κB2/p52 mediates enzalutamide resistance in castration-resistant prostate cancer cells, Endocr. Relat. Cancer 21 (2014) 435–442.
[7] E. Lavallée, et al., Increased prostate cancer glucose metabolism detected by 18f-fluorodeoxyglucose positron emission tomography/computed tomography in localised gleason 8–10 prostate cancers identifies very high–risk patients for early recurrence and resistance to castration, Eur. Urol. Focus 5 (2019) 998–1006.
[8] L. Stone, Mitochondrial metabolism: a target in AR-driven disease, Nat. Rev. Urol. (2019), https://doi.org/10.1038/s41585-018-0132-8, 16 1–1.
[9] K. Singh, et al., The pathophysiology and the therapeutic potential of cannabinoids in prostate cancer, Cancers 13 (2021) 4107.
[10] F.A. Javid, R.M. Phillips, S. Afshinjavid, R. Verde, A. Ligresti, Cannabinoid pharmacology in cancer research: a new hope for cancer patients? Eur. J. Pharmacol. 775 (2016) 1–14.
[11] L. de Petrocellis, et al., Non-THC cannabinoids inhibit prostate carcinoma growth in vitro and in vivo: pro-apoptotic effects and underlying mechanisms, Br. J. Pharmacol. 168 (2013) 79–102.
[12] A. Ligresti, et al., Antitumor activity of plant cannabinoids with emphasis on the effect of cannabidiol on human breast carcinoma, J. Pharmacol. Exp. Ther. 318 (2006) 1375–1387.
[13] A. Ligresti, L. de Petrocellis, V. di Marzo, From phytocannabinoids to cannabinoid receptors and endocannabinoids: pleiotropic physiological and pathological roles through complex pharmacology, Physiol. Rev. 96 (2016) 1593–1659.
[14] P. Morales, et al., Synthetic cannabinoid quinones: preparation, in vitro antiproliferative effects and in vivo prostate antitumor activity, Eur. J. Med. Chem. 70 (2013) 111–119.
[15] D. Roberto, L.H. Klotz, V. Venkateswaran, Cannabinoid WIN 55,212-2 induces cell cycle arrest and apoptosis, and inhibits proliferation, migration, invasion, and

tumor growth in prostate cancer in a cannabinoid-receptor 2 dependent manner, Prostate 79 (2019) 151–159.
[16] M. Cerasuolo, et al., Modeling acquired resistance to the second-generation androgen receptor antagonist enzalutamide in the TRAMP model of prostate cancer, Cancer Res. 80 (2020) 1564–1577.
[17] C. Morell, et al., The cannabinoid WIN 55,212-2 prevents neuroendocrine differentiation of LNCaP prostate cancer cells, Prostate Cancer Prostatic Dis. 19 (2016) 248–257.
[18] Myint, Z. et al. A phase I, dose-expansion cohort study on the safety of a cannabidiol for biochemical recurrence in prostate cancer patients. https://doi.org/10.1200/JCO.2021.39.6_suppl.TPS263 39, TPS263–TPS263 (2021).
[19] P.A. Kakimoto, J.D.C. Serna, V. de Miranda Ramos, A. Zorzano, A.J. Kowaltowski, Increased glycolysis is an early consequence of palmitate lipotoxicity mediated by redox signaling, Redox Biol. 45 (2021), 102026.
[20] N. Rimmerman, et al., Direct modulation of the outer mitochondrial membrane channel, voltage-dependent anion channel 1 (VDAC1) by cannabidiol: a novel mechanism for cannabinoid-induced cell death, Cell Death Dis. 4 (2013), e949.
[21] M. Olivas-Aguirre, et al., Cannabidiol directly targets mitochondria and disturbs calcium homeostasis in acute lymphoblastic leukemia, Cell Death Dis. 10 (2019) 1–19.
[22] R. Ronca, et al., Long-pentraxin 3 derivative as a small-molecule FGF trap for cancer therapy, Cancer Cell 28 (2015) 225–239.
[23] A. Ianevski, A.K. Giri, T. Aittokallio, SynergyFinder 2.0: visual analytics of multi-drug combination synergies, Nucleic Acids Res. 48 (2020) W488–W493.
[24] M. Solinas, et al., Cannabidiol inhibits angiogenesis by multiple mechanisms, Br. J. Pharmacol. 167 (2012) 1218–1231.
[25] Epidiolex (CBD) in Patients with Biochemically Recurrent Prostate Cancer - Full Text View - ClinicalTrials.gov. ⟨https://clinicaltrials.gov/ct2/show/NCT04428203⟩.
[26] G. Zadra, M. Loda, Metabolic vulnerabilities of prostate cancer: diagnostic and therapeutic opportunities, Cold Spring Harb. Perspect. Med. 8 (2018).
[27] B.J. Altman, J.C. Rathmell, Metabolic stress in autophagy and cell death pathways, Cold Spring Harb. Perspect. Biol. 4 (2012).
[28] J.G. Pastorino, J.B. Hoek, Regulation of hexokinase binding to VDAC, J. Bioenerg. Biomembr. 40 (2008) 171.
[29] D. Zhang, Y.M. Yip, L. Li, In silico construction of HK2-VDAC1 complex and investigating the HK2 binding-induced molecular gating mechanism of VDAC1, Mitochondrion 30 (2016) 222–228.
[30] D.J. Roberts, V.P. Tan-Sah, E.Y. Ding, J.M. Smith, S. Miyamoto, Hexokinase-II positively regulates glucose starvation induced autophagy through TORC1 inhibition, Mol. Cell 53 (2014) 521.
[31] R.B. Robey, N. Hay, Mitochondrial hexokinases, novel mediators of the antiapoptotic effects of growth factors and Akt, Oncogene 25 (2006) 4683–4696.
[32] X. Zhou, et al., Effect of PTEN loss on metabolic reprogramming in prostate cancer cells, Oncol. Lett. 17 (2019) 2856–2866.
[33] M. Wu, et al., Multiparameter metabolic analysis reveals a close link between attenuated mitochondrial bioenergetic function and enhanced glycolysis dependency in human tumor cells, Am. J. Physiol. Cell Physiol. 292 (2007) C125–C136.
[34] P. Chiodelli, et al., FGFR blockade by pemigatinib treats naïve and castration resistant prostate cancer, Cancer Lett. 526 (2022) 217–224.
[35] S.B. Shappell, et al., Prostate pathology of genetically engineered mice: definitions and classification. The Consensus Report from the Bar Harbor Meeting of the mouse models of human cancer consortium prostate pathology committee, Cancer Res. 64 (2004) 2270–2305.